Domain wall dynamics due to femtosecond laser-induced superdiffusive spin transport

Pavel Baláž,[1,2,*] Karel Carva,[1] Ulrike Ritzmann,[3,4] Pablo Maldonado,[3] and Peter M. Oppeneer[3,4]

[1]*Charles University, Faculty of Mathematics and Physics, Department of Condensed Matter Physics, Ke Karlovu 5, CZ 121 16 Prague, Czech Republic*

[2]*IT4Innovations Center, VSB Technical University of Ostrava, 17. listopadu 15, CZ 708 33 Ostrava-Poruba, Czech Republic*

[3]*Department of Physics and Astronomy, Uppsala University, Box 516, SE-75120 Uppsala, Sweden*

[4]*Department of Physics, Freie Universität Berlin, Arnimallee 14, D-14195 Berlin, Germany*

(Received 6 July 2019; revised manuscript received 22 April 2020; accepted 23 April 2020; published 14 May 2020)

Manipulation of magnetic domain walls via a helicity-independent laser pulse has recently been experimentally demonstrated and various physical mechanisms leading to domain wall dynamics have been discussed. Spin-dependent superdiffusive transport of hot electrons has been identified as one of the possible ways to affect a magnetic domain wall. Here, we develop a model based on superdiffusive spin-dependent transport to study the laser-induced transport of hot electrons through a smooth magnetic domain wall. We show that the spin transfer between neighboring domains can enhance ultrafast demagnetization in the domain wall. More importantly, our calculations reveal that when the laser pulse is properly focused onto the vicinity of the domain wall, it can excite sufficiently strong spin currents to generate a spin-transfer torque that can rapidly move the magnetic domain wall by several nanometers in several hundred femtoseconds, leading to a huge nonequilibrium domain wall velocity.

DOI: 10.1103/PhysRevB.101.174418

I. INTRODUCTION

Modern technologies such as magnetic memories or storage disks rely on the control and manipulation of magnetic bits. The ever-increasing demand for faster speed of magnetic recording continues to drive the interest in finding improved ways to control the magnetization dynamics, either by using magnetic fields, spin-current torques [1,2], thermal gradients [3–5], spin-orbit torques [6], or exchange-coupling torques [7]. These advanced methods allow the construction of a memory device based on manipulating domain walls [8]. The mutual interaction between light and magnetism has gained much attention in the last 20 years initiated by the discovery by Beaurepaire and coworkers [9] of ultrafast laser-induced demagnetization of Ni thin films. This phenomenon plays a dominant role, too, in the discussions on future magnetic devices. As a consequence, many related experimental studies have been carried out, leading to the discoveries of, e.g., the optical spin-transfer torque [10,11] and the optical spin-orbit torque [12].

From a theoretical point of view, different models and mechanisms were proposed to explain the ultrafast laser-induced demagnetization [9,13–20]. From those, it is important to emphasize two, namely, ultrafast demagnetization due to spin-flip relaxation [9,13–18] and nonlocal superdiffusive spin transport [19,20]. More specifically, within the latter, in the model introduced by Battiato, Carva, and Oppeneer [19,20] ultrafast demagnetization could be demonstrated without any additional assumptions for a spin-flip scattering mechanism. Importantly, the nonlocal character of this mechanism invoking spatial spin transport suggests that laser excitation can also be used to manipulate magnetic structures in magnetically nonhomogeneous systems [21–24]. For instance, it has been shown experimentally that the interplay between magnetic textures and ultrafast demagnetization can affect the domain structure in thin Co/Pt films on the subpicosecond timescale [25]. Additionally, it has been suggested that transfer of hot electrons flowing between different magnetic domains can accelerate the demagnetization process [26]. On the one hand, experimental observations on various samples indicate that this effect might be limited in some materials [27]. On the other hand, more recently laser-controlled manipulation of domain walls has been demonstrated in Co/Pt thin films [28], in Co/Cu/Ni trilayer films [29], and in $Co/Fe_{75}Gd_{25}$ bilayer films [30], as well as helicity-dependent domain wall motion [11], formation of vortices [31], and combination of laser-driven domain wall motion with the spin-Hall effect [32], and with currents [33].

In this paper, we study how superdiffusive spin currents can influence the magnetic texture, specifically, a thick magnetic domain wall. For simplicity we assume a one-dimensional model of an isolated magnetic domain wall separating two domains with opposite orientation of magnetization. Initially, we study demagnetization in a narrow magnetic domain wall to compare our results with previous studies [25]. Subsequently, we extend the study to wider and more realistic magnetic domain walls taking into account their detailed structure. To this end we generalized the model of superdiffusive spin-dependent transport for the study of noncollinear magnetic configurations. Our work reveals how a domain wall influences the flux of electrons along the sample and

*balaz@karlov.mff.cuni.cz

the demagnetization process. In more detail, we calculate the nonhomogeneous spin transfer torque acting on the domain wall and, consequently, study the dynamics of the magnetic moments. We show that when a femtosecond laser pulse is focused properly, it can trigger domain wall motion and shift the domain wall center with a very high out-of-equilibrium velocity of about 10^4 m/s.

The paper is organized as follows. In the following section we provide a short introduction to the superdiffusive spin-dependent transport model of hot electrons. In Sec. III we describe the generalization of the model for noncollinear magnetic textures. In Sec. IV we study the influence of the domain wall on ultrafast demagnetization. Second, in Sec. V we study ultrafast demagnetization and spin-transfer torque generation in wide magnetic domain walls. The laser-induced magnetization dynamics is studied as well. Finally, we discuss the consequences of our results in Sec. VI.

II. METHODS

The superdiffusive spin-dependent transport model [19,20] is based on the distinct transport behavior of minority and majority electrons due to their different velocities and lifetimes. The starting point of the superdiffusive spin-dependent transport model of hot electrons [19,20] is the excitation of localized electrons above the Fermi level (usually from d to s band) induced by a femtosecond laser pulse. Because of the higher electron velocities the excited hot electrons are treated as itinerant particles moving along the sample [34]. Motion of the itinerant electrons is described by a transport equation taking into account electron spins, $\sigma \in \{\uparrow, \downarrow\}$, and energies, ϵ. The electron velocities, $v_\sigma(\epsilon)$, and lifetimes, $\tau_\sigma(\epsilon)$, depend on these quantities. Due to the difference of $v_\uparrow$ ($\tau_\uparrow$) and $v_\downarrow$ ($\tau_\downarrow$) in a magnetic material, the current of flowing electrons gets polarized. In case of multilayers, spin filtering via multiple spin-dependent reflections at the interfaces contributes to the spin current polarization [34]. As a result, loss of the magnetic momentum carried away by the spin currents is observed as a local demagnetization of the magnetic material illuminated by the laser pulse. Due to high electron velocities, this demagnetization process happens on a femtosecond timescale. Note that this model assumes purely nonthermal laser excitation of electrons without any effects of temperature [35]. Importantly, the spin transport of the hot electrons is neither purely ballistic nor diffusive. Its transport character is changing in time from initially ballistic motion toward diffusive motion via the superdiffusive regime, which takes between 500 fs up to 1 ps depending on the laser pulse and material properties [20]. Consequently, the model is not intended to treat electrons near the Fermi level or even equilibrium spin currents [36,37], where more suitable tools are available.

The model has been supported by a number of experimental observations [22,23,38–42]. Alternatively, the theory of spin-dependent transport of hot electrons has been formulated in the framework of the Boltzmann transport equation [43] showing that the energy dependence of the injected hot electrons plays a crucial role for the spin transport.

So far, the superdiffusive transport model has been mostly used to explain ultrafast demagnetization processes, especially in single magnetic layers and collinear magnetic multilayers. However, in the case of noncollinear magnetic configuration the spin currents generated by the superdiffusive spin-dependent transport of hot electrons can induce spin-transfer torques [1,2,44–48] acting on the magnetic moments and, consequently, magnetization dynamics [49]. Such a noncollinear magnetic configuration can be achieved in magnetic multilayers or in magnetic films or wires featuring magnetic textures such as domain walls, magnetic bubbles, or skyrmions.

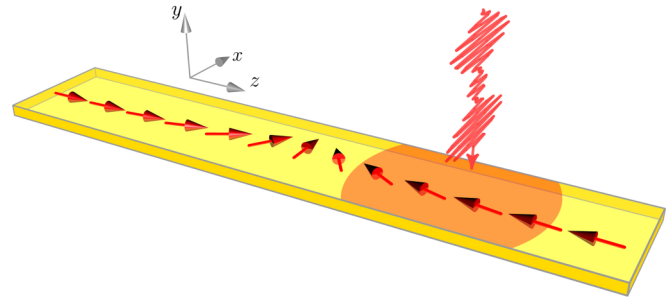

FIG. 1. Sketch of a head-to-head magnetic domain wall and the used coordination system. The wave vector of the incident laser beam is aligned with the y axis.

Recently, we developed an effective model for the spin-transfer toque induced by hot electrons in noncollinear spin valves [50]. It has been shown that, in accord with experimental observations [21–24], excitation of hot electrons in one magnetic layer can lead to a fast spin-transfer torque and small-angle magnetization precessions in the second magnetic layer even though both magnetic layers are separated and magnetically decoupled by a nonmagnetic one. Here, we adopt a different approach where we take into account spin rotation between neighboring magnetic moments in a magnetic domain wall. The spin-dependent transport properties inside the domain wall are then included in the transmissions and reflections between discretization cells with uniform magnetizations as described below in Sec. III A.

III. THEORETICAL MODEL

We start with the investigation of laser-induced magnetization dynamics of a 1-dimensional wire of length $L = N\Delta z$, where Δz is a spatial discretization length and N is the number of cells in the simulation, which simulates a domain wall. The domain wall is located in the middle of the wire, where $z = z_c$. We illustrate the domain wall schematically in Fig. 1.

We assumed that the magnetization is varying along the z axis. In equilibrium the magnetization vector is given by $\boldsymbol{M}(z) = M_0\,\hat{\boldsymbol{m}}(z)$, where M_0 is the saturated magnetization and $\hat{\boldsymbol{m}}(z)$ is a unit vector

$$\hat{\boldsymbol{m}}(z) = (\cos\phi \sin\theta(z), \sin\phi \sin\theta(z), \cos\theta(z)), \qquad (1)$$

where ϕ is constant with respect to z, and

$$\theta(z) = 2\arctan\left[\exp\left(\frac{z - z_0}{\Delta}\right)\right], \qquad (2)$$

with z_0 the position of the domain wall center [51,52]. Δ is the domain wall width given by

$$\Delta = \sqrt{A_{\rm ex}/K_{\rm u}}, \tag{3}$$

with $A_{\rm ex}$ being the exchange stiffness and $K_{\rm u}$ is the uniaxial anisotropy constant [51,52]. Equation (2) describes a head-to-head magnetic domain wall separating the left magnetic domain with magnetization $\hat{\boldsymbol{m}}_{\rm L} = \hat{\boldsymbol{e}}_z \equiv (0, 0, 1)$ from the right one $\hat{\boldsymbol{m}}_{\rm R} = -\hat{\boldsymbol{e}}_z$.

For our specific 1-dimensional wire, we assume $\phi = \pi/2$ (the magnetization is in the layer's plane). Thus the magnetization in the ith cell reads $\hat{\boldsymbol{m}}_i = (\sin\theta_i, 0, \cos\theta_i)$, see Fig. 1, and the magnetization direction $\theta_i \equiv \theta(z_i)$ becomes

$$\theta_i = 2\arctan\left[\exp\left(\frac{z_i - z_{\rm c}}{\Delta}\right)\right], \quad i = 1, 2, \ldots, N, \tag{4}$$

where z_i is the position of the ith cell.

A. Electronic transport

The transport process in the modeled system consists of two effects. There is spin-dependent scattering described by the superdiffusive model, and also the response of electrons to the varying quantization axis. Both these effects represent a perturbation of the total electron transport, and we treat them separately in each discretization cell. The error due to their separation will be comparable to the error of the discretization itself, and thus negligible as long as the discretization cell is small enough. This allows us to describe transport within each cell by the two-current model, while the transition between cells is described by the more general formalism described below.

In each discretization step scattering takes place. Full description of this process including reflections at interfaces is rather complex, and we follow here methods of the superdiffusive transport model described in Ref. [34]. Two-channel components of the right-going current in the ith cell are denoted as $\overrightarrow{J_{\sigma(i)\xi}}$, where $i = 1, 2, \ldots, N-1$. The extra index ξ can have values either $\xi = (-)$ for the current on the left side of the cell or $\xi = (+)$ for that on the right side. For a right-going current these correspond to currents before and after the influence of possible scattering in the cell, $\overrightarrow{J_{\sigma(i)(-)}}$ and $\overrightarrow{J_{\sigma(i)(+)}}$. This current is thus obtained from the quantity Φ described in Eq. (24) of Ref. [34].

The quantization axis is in each discretization cell aligned along the local magnetization, $\hat{\boldsymbol{m}}_i$. The spin current leaving the ith cell is oriented along $\hat{\boldsymbol{m}}_i$ and enters the cell whose magnetization is oriented along $\hat{\boldsymbol{m}}_{i+1}$. Its magnitude is obtained from $\overrightarrow{J_{\sigma(i)(+)}}$. We assume that electrons respond to the magnetization variation within each discretization cell by aligning its quantization axis to the cell direction, as already employed in other studies of torque in domain walls [53]. This alignment is equivalent to absorption of the spin current component transverse to that cell. This absorption typically takes place within less than 1 nm from the interface [54]—a distance smaller than the simulation cell—and gives rise to a torque (see below). Inside any ith cell we thus consider only the projection of conduction electron spins into the $\hat{\boldsymbol{m}}_i$ direction as contributing to the spin current before scattering, which can then be expressed using the simple two-channel current $\overrightarrow{J_{\sigma(i)(-)}}$. In this way we formally localize the effect of the spin quantization axis change on the transport always into the interface between cells, while the effect of scattering is separated and takes place inside cells.

In contrast to ultrathin atomic domain walls [55], which can lead to a significant electron scattering due to the strong spatial variation of the magnetization [56,57], we inspect here thick domain walls with moderate variation of magnetization direction. In this case, the effect of reflecting electrons is negligible [58]. As long as the domain wall width is much larger than the electron wavelength the total transmission of electrons through the domain wall is close to 1 [57]. The magnetization rotation rate of domain walls that we considered is smaller than 0.03 per lattice constant, and thus satisfies this condition. Therefore, we do not assume any reflection of electrons from the domain wall or inside it.

As a consequence of the magnetization direction change between the $(i-1)$th and ith cell the local quantization axis of an electron moving from the $(i-1)$th cell to the ith one is changed by an angle $\delta\theta^{(i)} = \theta_i - \theta_{i-1}$. Thus, regardless of the electron flow direction, the currents in the $(i-1)$th cell can be expressed in the local frame of the ith one as $\hat{\jmath}'_{(i-1)\xi} = \hat{U}_i\, \hat{\jmath}_{(i-1)\xi}\, \hat{U}_i^{\dagger}$, where

$$\hat{\jmath}_{(i-1)\xi} = \begin{pmatrix} j_{\uparrow(i-1)\xi} & 0 \\ 0 & j_{\downarrow(i-1)\xi} \end{pmatrix}, \tag{5}$$

and $\hat{U}_i$ is the spin-space transformation unitary matrix due to the rotation by the angle $\delta\theta^{(i)}$ in the x-z plane:

$$\hat{U}_i = \begin{pmatrix} \cos\left(\delta\theta^{(i)}/2\right) & -\sin\left(\delta\theta^{(i)}/2\right) \\ \sin\left(\delta\theta^{(i)}/2\right) & \cos\left(\delta\theta^{(i)}/2\right) \end{pmatrix}. \tag{6}$$

This leads to the following transformation of the two-channel current for electrons moving from the $(i-1)$th cell to ith cell:

$$\overrightarrow{J_{\sigma(i)(-)}} = \sum_{\sigma'} T^{(i)}_{\sigma\sigma'} \cdot \overrightarrow{J_{\sigma'(i-1)(+)}}. \tag{7}$$

The effective interface transmission matrix between the ith and $(i+1)$th cell is given by

$$T^{(i)} = \begin{pmatrix} T^{(i)}_{\uparrow\uparrow} & T^{(i)}_{\uparrow\downarrow} \\ T^{(i)}_{\downarrow\uparrow} & T^{(i)}_{\downarrow\downarrow} \end{pmatrix}, \tag{8}$$

where

$$T^{(i)}_{\uparrow\uparrow} = T^{(i)}_{\downarrow\downarrow} = \cos^2\left(\delta\theta^{(i)}/2\right), \tag{9a}$$

$$T^{(i)}_{\uparrow\downarrow} = T^{(i)}_{\downarrow\uparrow} = \sin^2\left(\delta\theta^{(i)}/2\right). \tag{9b}$$

The transmission matrix (8) applies for electrons moving in both directions. Similarly, for the current moving from right to left we can write

$$\overleftarrow{J_{\sigma i(+)}} = \sum_{\sigma'} T^{(i+1)}_{\sigma\sigma'} \cdot \overleftarrow{J_{\sigma'(i+1)(-)}}. \tag{10}$$

Note that the currents in Eqs. (7) and (10) are taken at the same energy level ϵ_j. We assume that electrons flowing through an interface do not change their energy.

B. Spin-transfer torque

As argued above, the orientation of spin current is along $\hat{\boldsymbol{m}}_i$ on both the (+) and (−) side of the ith cell. Then we define the spin current of right-moving electrons in the ith cell as a sum of contributions from energy levels in the superdiffusive model:

$$\overrightarrow{\boldsymbol{J}_{s\,(i)\,\xi}} = \frac{\hbar}{2\,e}\sum_{j=1}^{N_\epsilon}\left[\overrightarrow{J_{\uparrow\,(i)\,\xi}}(\epsilon_j) - \overrightarrow{J_{\downarrow\,(i)\,\xi}}(\epsilon_j)\right]\hat{\boldsymbol{m}}_i, \tag{11}$$

where N_ϵ is the number of energy levels assumed in the calculations. Similarly, we can define spin currents flowing from the right to the left:

$$\overleftarrow{\boldsymbol{J}_{s\,(i)\,\xi}} = \frac{\hbar}{2\,e}\sum_{j=1}^{N_\epsilon}\left[\overleftarrow{J_{\uparrow\,(i)\,\xi}}(\epsilon_j) - \overleftarrow{J_{\downarrow\,(i)\,\xi}}(\epsilon_j)\right]\hat{\boldsymbol{m}}_i. \tag{12}$$

It is important to note that by definition, currents of electrons moving from the left to the right, $\overrightarrow{J_{\sigma\,(i)\,\xi}}(\epsilon_j)$, have positive sign while the currents moving from the right to the left, $\overleftarrow{J_{\sigma\,(i)\,\xi}}(\epsilon_j)$, have negative sign.

Spin transfer torque acting on the magnetization in the ith cell corresponds to the change of the transverse part of the spin current (with respect to $\hat{\boldsymbol{m}}_i$) when passing through the cell. Furthermore we assume that the transverse part is completely absorbed in the cell, in agreement with other approaches to domain walls [53]. Therefore only the value of transverse current entering the cell contributes to the torque. One possible way to obtain the transverse part of the incoming current is to subtract the longitudinal part. Taking into account Eqs. (7) and (9) we find that

$$\left|\overrightarrow{\boldsymbol{J}_{s\,(i)\,(-)}}\right| = \left|\overrightarrow{\boldsymbol{J}_{s\,(i-1)\,(+)}}\right|\,\cos\left(\delta\theta^{(i)}\right), \tag{13}$$

which shows that $\overrightarrow{\boldsymbol{J}_{s\,(i)\,(-)}}$ is exactly the longitudinal component of $\overrightarrow{\boldsymbol{J}_{s\,(i-1)\,(+)}}$ (with respect to $\hat{\boldsymbol{m}}_i$). This leads to the following formula for the torque due to the right-going current entering the ith cell [44,48]:

$$\overrightarrow{\boldsymbol{\tau}_i} = \overrightarrow{\boldsymbol{J}_{s\,(i-1)\,(+)}} - \overrightarrow{\boldsymbol{J}_{s\,(i)\,(-)}}, \tag{14}$$

Similarly, from left-moving electrons we obtain

$$\left|\overleftarrow{\boldsymbol{J}_{s\,(i)\,(+)}}\right| = \left|\overleftarrow{\boldsymbol{J}_{s\,(i+1)\,(-)}}\right|\,\cos\left(\delta\theta^{(i+1)}\right), \tag{15}$$

$$\overleftarrow{\boldsymbol{\tau}_i} = \overleftarrow{\boldsymbol{J}_{s\,(i+1)\,(-)}} - \overleftarrow{\boldsymbol{J}_{s\,(i)\,(+)}}. \tag{16}$$

As a consequence of Eqs. (14) and (15), for the magnitudes of the local torques we also obtain

$$|\overrightarrow{\boldsymbol{\tau}_i}| = \left|\overrightarrow{\boldsymbol{J}_{s\,(i-1)\,(+)}}\right|\,\sin\left(\delta\theta^{(i)}\right), \tag{17a}$$

$$|\overleftarrow{\boldsymbol{\tau}_i}| = \left|\overleftarrow{\boldsymbol{J}_{s\,(i+1)\,(-)}}\right|\,\sin\left(\delta\theta^{(i+1)}\right). \tag{17b}$$

Note that this dependence on the rate of magnetization angle change actually represents a special case of the general dependence on $\nabla\hat{\boldsymbol{m}}$ derived elsewhere by Li and Zhang [59].

Finally, the total spin torque acting on ith magnetization is given by

$$\boldsymbol{\tau}_i = \overrightarrow{\boldsymbol{\tau}_i} + \overleftarrow{\boldsymbol{\tau}_i}. \tag{18}$$

For the sake of clarity, in the definitions (11)–(18) we omitted the time dependence of the electron currents. The magnetizations directions, $\hat{\boldsymbol{m}}_i$, are assumed to be constant in the transport calculations.

C. Magnetization dynamics

To study the magnetization dynamics of the magnetic cells we use the Landau-Lifshitz-Gilbert equation (LLG), which for the ith magnetic moment in the wire reads

$$\frac{d\hat{\boldsymbol{m}}_i}{dt} - \alpha\,\hat{\boldsymbol{m}}_i \times \frac{d\hat{\boldsymbol{m}}_i}{dt} = \boldsymbol{\Omega}_i, \tag{19}$$

where $\gamma = |\gamma_{\rm g}| > 0$ is the gyromagnetic ratio, t is time, α is the Gilbert damping parameter, and $\boldsymbol{\Omega}_i$ is the overall torque acting on the ith local magnetization defined as

$$\boldsymbol{\Omega}_i = -\mu_0\,\gamma\,\hat{\boldsymbol{m}}_i \times \boldsymbol{H}_{\rm eff}^{(i)} + \frac{1}{\mu_0\,M_i^2\,V_{\rm cell}}\,\boldsymbol{\tau}_i, \tag{20}$$

which consists of a part induced by the effective magnetic field, $\boldsymbol{H}_{\rm eff}^{(i)}$, and the spin-transfer torque term containing $\boldsymbol{\tau}_i$, where M_i is the magnitude of magnetization in the ith computational cell, and $V_{\rm cell}$ is the cell volume. Here, it is important to mention that the magnitude M_i depends on the superdiffusive transport and changes in time [19]. Equation (20) shows that spin-transfer torque is stronger when acting on a localized magnetic moment.

Generally, the effective magnetic field is defined as a functional derivative of total volume energy density, w,

$$\boldsymbol{H}_{\rm eff}^{(i)} = \frac{1}{\mu_0 M_0}\frac{\delta w(z_i)}{\delta\hat{\boldsymbol{m}}_i}, \tag{21}$$

where μ_0 is vacuum permeability, M_0 is the equilibrium value of the saturated magnetization, and z_i is the position of the ith cell. The energy density of the total volume reads

$$w(z) = A_{\rm ex}\left(\frac{\partial\theta(z)}{\partial z}\right)^2 + K_{\rm u}\,\cos^2\theta(z) + K_\perp[\cos\phi\,\sin\theta(z)]^2, \tag{22}$$

where $K_{\rm u}$ is the uniaxial anisotropy constant and $K_\perp$ is the perpendicular out-of-plane anisotropy constant. The spin-transfer torque, $\boldsymbol{\tau}_i$, is given by Eq. (18).

IV. NARROW MAGNETIC DOMAIN WALL

We apply the above described model to study the spin-dependent transport in a simplified system of a narrow magnetic domain wall to investigate the effects of a femtosecond laser pulse on magnetic domains walls formed typically in multilayers like Co/Pt or Co/Pd having a strong out-of-plane magnetic anisotropy [25–27].

In this case we focus on the effects of the superdiffusive transfer on the domain wall structure. Thus we use first a simplified model of a sharp domain wall, where the magnetization direction is changed abruptly by 180°, which reproduces the experimental conditions. Hot electrons passing the domain wall move from being in the majority to being in the minority spin channel and vice versa. As a result, spins accumulate in the vicinity of the domain wall causing a change of the domain wall profile [60]. No spin flips or reflections were assumed at the domain wall.

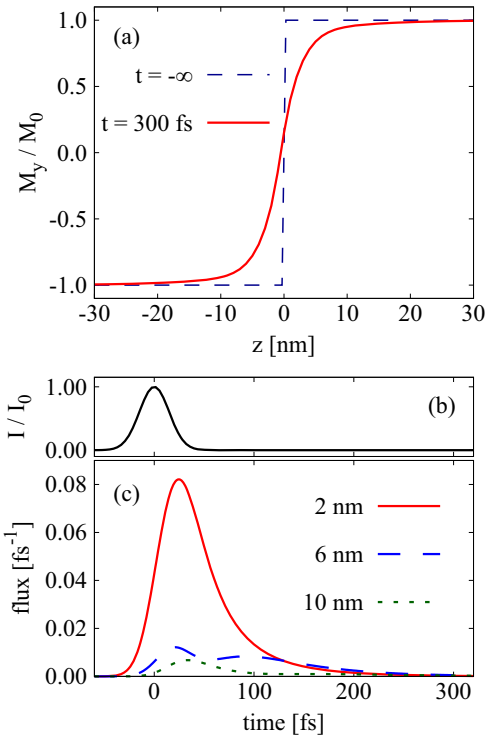

FIG. 2. Superdiffusive transport through a narrow magnetic domain wall. (a) Dashed (blue) line shows out-of-plane component of magnetization in the vicinity of a narrow magnetic domain wall in the equilibrium ($t = -\infty$). Solid (red) line shows the out-of-plane magnetic component 300 fs after the maximum of the laser pulse. (b) Time variation of Gaussian laser pulse intensity with peak at time $t = 0$ and FWHM 35 fs. (c) Corresponding time variation of the spin fluxes calculated for different distances (2, 6, and 10 nm) from the domain wall.

In our calculations we assumed a sample as long as 100 nm with spatial discretization $\Delta z = 1$ nm. Moreover, we assumed time discretization $\Delta t = 1$ fs. For simplicity, we used the electron velocities and lifetimes of hot electrons calculated for Fe [61]. For the electronic transport we assumed $N_\epsilon = 12$ energy levels above the Fermi energy. The difference between the subsequent energy levels was $\Delta\epsilon = 0.125$ eV, which allows us to cover an energy range up to 1.5 eV. We assumed that the whole sample was homogeneously excited by the laser pulse having a Gaussian shape with maximum in $t = 0$ and full width in half maximum $t_p = 35$ fs; see Fig. 2(b). Altogether this pulse excites 0.2 electrons at each energy/spin level, which corresponds to a laser fluence $F = 2.6$ mJ/cm^2.

In Fig. 2(a) we show the effect of the femtosecond spin pulse on the domain wall by locating the sharp step domain wall at $z = 0$. The dashed (blue) line shows the equilibrium distribution of the out-of-plane magnetization component along the sample normalized to the equilibrium saturated magnetization M_0. In turn, the solid (red) line describes the out-of-plane magnetization 300 fs after the laser pulse intensity reached its maximum. The boundary between the domains has become smeared due to ultrafast demagnetization caused by the superdiffusive spin transport between the neighboring magnetic domains. The hot electrons excited by the laser pulse move along the sample and carry the angular momentum. Because the velocities of electrons in spin-up and spin-down channels differ, spin accumulation builds up in the vicinity of the domain wall. As a result, the domain wall profile becomes smeared. Figure 2(a) shows that the spin accumulation decays as a function of the distance from the domain wall center and reaches up to about 20 nm. This result is in good agreement with experimental observations and Monte Carlo simulations reported by Pfau *et al.* [25].

The timescale of the ultrafast demagnetization is shown in Figs. 2(c), which illustrates the time variation of the total spin flux taken at different distances from the domain wall. The amplitude of the spin flux strongly decreases with the distance from the domain wall. Especially, temporal dependencies of more remote fluxes exhibit more than one peak. This is a result of the secondary electrons which are generated by the avalanches during the scattering of the hot electrons. Importantly, the out-of-equilibrium spin fluxes become zero after about 300 fs from the laser pulse, indicating the timescale of the ultrafast demagnetization.

V. WIDE MAGNETIC DOMAIN WALL

In the following, we present our numerical results for a wider domain wall with a detailed structure of the domain wall profile as described by Eq. (2). In our calculations we assumed a wire as long as 200 nm. With spatial discretization $\Delta z = 1$ nm we used $N = 200$ computational cells. The excited electrons can occupy $N_\epsilon = 12$ energy levels above the Fermi energy with energy discretization $\Delta\epsilon = 0.125$ eV. The energy and spin-resolved electron velocities and lifetimes used in our calculations correspond to those of iron as calculated by *ab initio* methods [20,61,62].

Moreover, in all our simulations we assume a Gaussian laser pulse of length $t_p = 35$ fs. During its duration, this pulse excites the same number of electrons on each energy and spin level. When considering the laser fluence $F \simeq 12.8$ mJ/cm^2 we obtain 1 excited electron on each energy/spin level in each 1-nm-wide discretization cell.

A. Ultrafast demagnetization

First, we focus on the ultrafast demagnetization induced by the laser pulse. Here, we assume that the whole sample is excited homogeneously. Therefore, the same number of electrons is excited by the laser pulse in each computational cell. This situation corresponds to a case where the laser spot exceeds the size of the computational length of the wire, L. In our analysis, we focus on the central part of the wire, which is far from its boundaries. In the case of a uniformly magnetized sample, the same number of electrons are flowing in both directions in the center of the wire. Thus, no demagnetization in the here-considered 1D transport model can be obtained. Oppositely, when a domain wall of width Δ is located in the center of the wire, electrons flowing through the domain wall from the left to the right are polarized in the left magnetic domain, while the electrons moving in the opposite direction are polarized in the right magnetic domain. Thus the left and right spin fluxes have opposite polarizations. As a result, partial demagnetization at the position of the domain wall

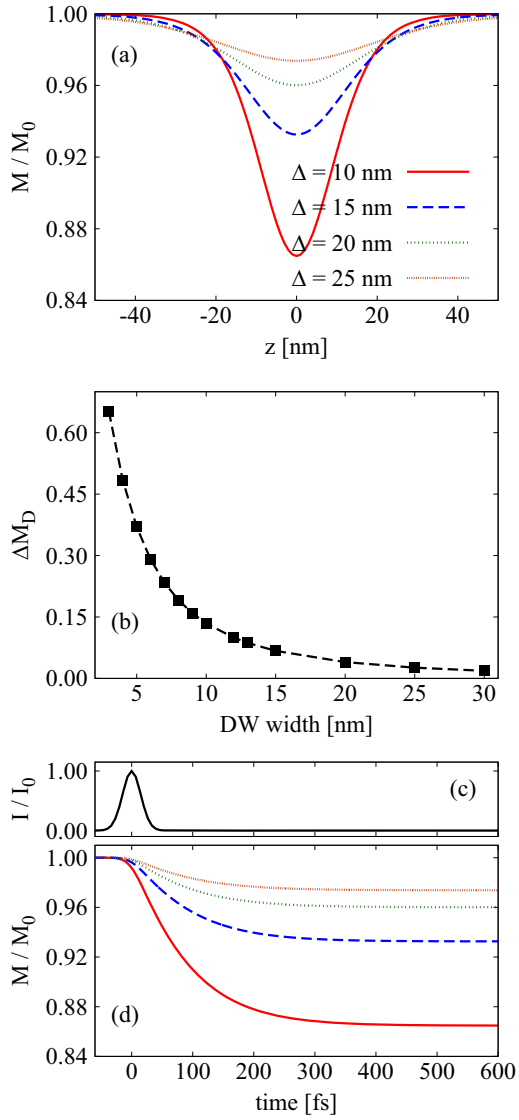

FIG. 3. Laser-induced demagnetization in the vicinity of the domain wall calculated for various DW widths. (a) Spatial dependence of magnetization taken 1 ps after the pulse. (b) Demagnetization in the DW center, $z = 0$, taken 1 ps after the pulse as a function of the DW width. (c) Time variation of Gaussian laser pulse intensity with peak at time $t = 0$ and FWHM 35 fs. (d) Time dependence of magnetization in the DW center after the laser pulse, for various DW widths. The lines correspond to those shown in (a).

(DW) and its vicinity can be expected. This mechanism is the same as the one described above for the narrow DW. Figure 3(a) shows the magnetization profile as function of the distance with respect to the central part of the wire taken 1 ps after the laser pulse for various DW widths: $M_D(z) = M(t = 1\,\text{ps}, z)$. We observe that the maximum demagnetization, $\Delta M_D = 1 - M_D/M_0$, is observed in the center of the domain wall and decreases toward zero deeper in the domains. Since the electronic transport is limited by the lifetimes of s electrons, the demagnetization becomes less pronounced for wider domain walls. Figure 3(b) shows how the maximum demagnetization in the DW center, $z = 0$, changes as a function of the DW width. This reflects the fact that the demagnetization is governed by the spin transport between magnetic domains with opposite magnetizations.

Additionally, we focus on the time dependence of the demagnetization process. Figure 3(b) shows the time dependence of the magnetization in the DW center, $z = 0$. In this point we define the demagnetization time τ_D as a time when the local magnetization $M(t)$ reaches $M(\tau_D) = (1 - e^{-1})(M_0 - M_D)$. This demagnetization time has been found to be virtually the same for all the studied DW thicknesses, $\tau_D \simeq 145$ fs.

It is important to note that in a realistic system, when excited electrons move in all three directions, demagnetization due to interdomain spin transport will appear as an effect additional to the demagnetization, which might be observed also in samples with uniform magnetization.

B. Spin-transfer torque

When a magnetic domain wall is located in the middle of the sample, which is uniformly excited by a laser pulse, the equal flow of electrons in both directions leads to zero total spin-transfer torque acting on the domain wall. Hence, no net domain wall motion can be expected due to a laser excitation in a symmetric system. To obtain a nonzero spin-transfer torque, one needs to create asymmetry in the left and right electron fluxes. This can be accomplished by a number of different ways using electric or thermal gradients, employing different materials, or by changing magnetic topology in the sample creating additional magnetic textures. Most of these methods, however, exert an additional torque on the magnetic domain wall. Therefore, here we study a simplified model, by assuming that the hot electrons are excited by the laser pulse only in a certain restricted region of the sample of width l_{ex}. We also assume that electrons are excited homogeneously by the laser pulse. Significantly, we observe that the spin density and spin fluxes in the domain wall depend on the distance of the excitation region from the domain wall, and therefore extend our study to investigate how the spin-transfer torque acting on the domain wall can be manipulated changing the position of the excitation region along the sample. Consequently, we explore domain wall dynamics excited by the spin-transfer torque of superdiffusive hot electrons.

To inspect the generation of the spin-transfer torque by the laser pulse, we assume that the domain wall is located in the middle of the sample, $z = 0$. The laser pulse excites hot electrons in the excitation region. Part of the hot electrons pass the domain wall and the spin flow locally generates spin-transfer torque due to magnetization variation. The spin-transfer torque is proportional to the local transverse spin current as given by Eq. (18).

Figure 4 shows the space-time maps of the spin-transfer torque in the neighborhood of the domain wall. The DW width is $\Delta = 10$ nm and the width of the excitation region is assumed to be $l_{ex} = 40$ nm. The temporal profile of the laser beam intensity used in the calculations is shown in Fig. 4(a). Figure 4(b) depicts a situation when the excitation region is symmetric with respect to the domain wall center. Importantly, the spin-transfer torque in the center of the domain wall remains zero all the time. Conversely, on both sides of the domain wall the spin torque is nonzero and changes in

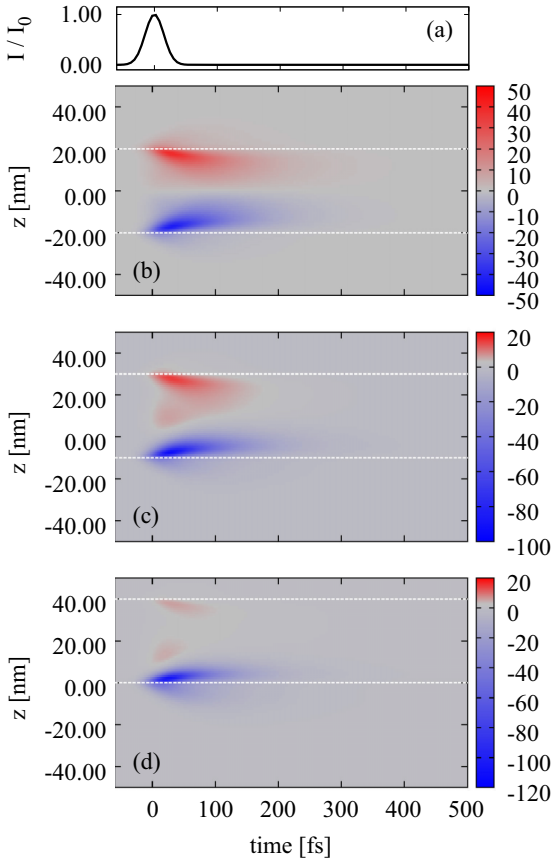

FIG. 4. Spatial and temporal dependence of the transverse spin current in the neighborhood of a domain wall in the units of $[M_0/M(z)][\hbar/(2e)]$ fs^{-1}. The domain wall center is located at $z = 0$ and its width is $\Delta = 10$ nm. The excitation region is restricted to the area between the white dashed lines. (a) Time variation of Gaussian laser pulse intensity with peak at time $t = 0$ and FWHM 35 fs. (b) The excitation region is symmetric with respect to the position of the domain wall center. (c) and (d) The excitation region is asymmetric with respect to the position of the domain wall center. In case (d) the borderline of the excitation region passes through the domain wall center.

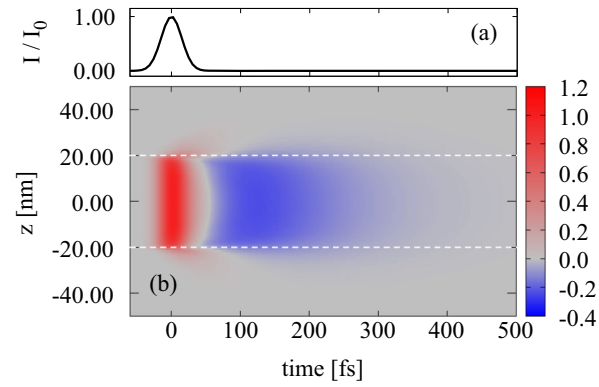

FIG. 5. Spatial and temporal dependence of a laser-induced charge current in the neighborhood of the domain wall, given in units of particles per fs. The parameters of the calculations are the same as in Fig. 4(b). Panel (a) shows the time variation of the Gaussian laser-pulse intensity.

time. This torque is nonuniform in space and varies in time. Its variation is caused by both position dependence of the magnetization gradient across the domain wall as well as spin relaxation. Due to the symmetry of the system, the spatial dependence of the spin-transfer torque remains antisymmetric. The spin-transfer torque decreases in time; the total time in which the spin torque is acting on the magnetic moments is about ∼500 fs.

The situation is different when the center of the excitation region is shifted from the DW center. This is shown in Figs. 4(c) and 4(d), which depict the transverse spin current when the center of the excitation region is shifted from the domain wall center by 10 and 20 nm, respectively. In both cases we observe asymmetry of the spin currents on the right and left hand side of the domain wall. As a result, the spin torques acting in the domain wall become strongly asymmetric. Figure 4(d) shows a specific case, where one of the borderlines of the excitation region is located at the DW center. Thus, electrons are excited by the laser pulse just in one half of the domain wall. The dominant spin-transfer torque is generated in the vicinity of the domain wall center at the borderline of the excitation region.

Summarizing, Fig. 4 illustrates that a symmetric DW excitation leads to zero total spin-transfer torque and no domain wall motion. Additionally, as the center of the excitation region departs from the DW center, the asymmetry of the spin torque increases, and as a result magnetization dynamics is expected. This magnetization dynamics can possibly lead either to a deformation of the domain wall structure or to a domain wall motion. A combination of both effects is also possible.

In addition, Fig. 5 shows the spatial and temporal variation of the laser-induced charge current in the neighborhood of the DW, in units of number of particles per fs. The charge current has been estimated from the time derivative of the number of electrons in each computational cell. Thus, a positive charge current means an increase of the number of electrons while a negative one signalizes decay of the charge accumulation. Figure 5 shows a rapid increase of the charge current in the excitation region after the laser pulse. When the laser beam dies out the charge accumulation starts to decay. In contrast to the spin current, the charge current profile does not depend on the position of the excitation region with respect to the DW center. The maximum charge current density reaches values of about 10^{15}–10^{16} A/m^2. These values are a few orders of magnitude higher than usual current densities used in standard spin-torque experiments [63]. However, the time duration of the charge current pulse is limited to a small timescale of a few tens of femtoseconds. Therefore, any detrimental effects of the Joule heating can be neglected.

In the previous section we have shown that laser-induced spin transport between the domains can reduce the magnetization by about 20%. Such a reduction of magnetization can affect both the local effective fields acting on the localized magnetic moment and the spin-transfer torque. The response of the magnetization dynamics to the variation of an effective magnetic field in ferromagnets will happen on a nanosecond scale, which is definitely longer than the domain wall

dynamics induced by superdiffusive spin-transfer torque. For this reason we do not assume a magnetization reduction in the effective magnetic field, but this effect is included in the spin-torque term. Similarly, in our simulations we disregard effects connected with temperature gradients or change of the magnetic anisotropy.

C. Domain wall dynamics

By using the LLG model [Eq. (19)] we study how the spin-transfer torque influences the magnetization dynamics. We start our simulations from a static configuration with a head-to-head magnetic domain wall located in the center of the sample. Magnetic moments completely lie in the plane of the sample. The magnetization dynamics starts with the 35 fs laser pulse leading to a time-dependent spin torque acting on the localized magnetic moments in the chain.

In our simulations we have assumed an equilibrium saturated magnetization $M_0 = 1.7 \times 10^6$ A/m, exchange stiffness $A_{ex} = 2 \times 10^{-11}$ J/m^3, and no applied magnetic field. The width of the magnetic domain wall will be modified by the uniaxial magnetic anisotropy, K_u, which obeys Eq. (3). The distance between the localized magnetic moments is in agreement with the discretization in the spin transport calculations, i.e. $a = 1$ nm. Finally, the Gilbert damping parameter $\alpha = 10^{-3}$ has been assumed.

In our simulations we assume that the magnetization dynamics will be small enough and will not substantially influence the flow of electrons. Therefore, we can separate the simulation of magnetization dynamics from the ones of superdiffusive spin-dependent transport.

Initially, our simulations reveal that the laser pulse primarily causes a shift of the center of the magnetic domain wall without any substantial modification of the DW profile or magnetization tilting. This simplifies the description of the DW dynamics to the time dependence of the DW center position. Therefore, in Fig. 6(b) we show the time evolution of the DW center after the laser pulse is applied. Different curves correspond to different positions of the excitation region. The position of the excitation region, z_{ex}, is given by its center with respect to the initial position of the DW center. In all our calculations the length of the excitation region is $l_{ex} = 40$ nm. After the pulse is applied, the domain wall starts to move. It stops after about 500 fs, which corresponds to the time when the spin fluxes diminish. Importantly, the DW displacement caused by one laser pulse strongly depends on the position of the excitation region. This means that also the DW velocity depends on z_{ex}.

Figure 6(c) shows how the DW displacement depends on the position of the excitation region. To this end we show the DW position 1 ps after the laser pulse maximum when its dynamics completely stopped. The dependence is shown for various DW widths. The plot shows nonmonotonic dependence of DW displacement on z_{ex} revealing a number of properties. We observe that, for all values of Δ, DW displacement remains zero for a symmetric electron excitation when $z_{ex} = 0$. This is caused by zero total spin-transfer torque produced in the symmetric case, as explained by Fig. 4(b). Besides, as the center of the excitation region departs from the DW center, the absolute value of the DW displacement

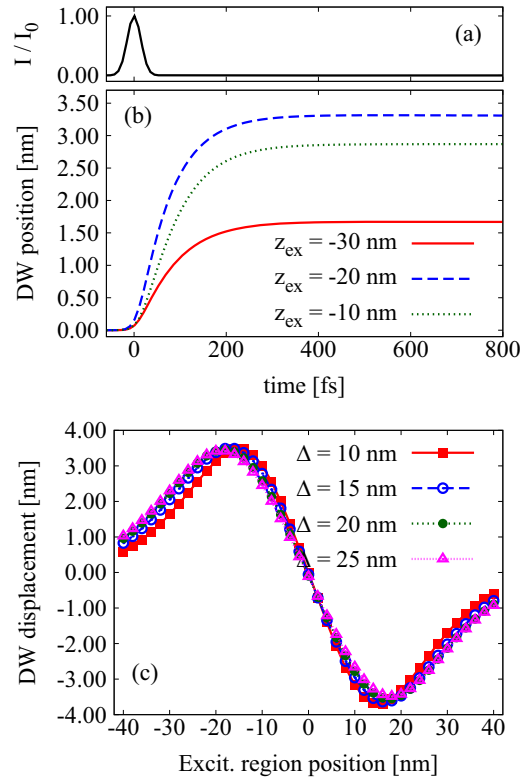

FIG. 6. Laser-induced dynamics of the domain wall. (a) Time variation of Gaussian laser pulse intensity with peak at time $t = 0$ and FWHM 35 fs. (b) Time dependence of the domain wall position after the laser pulse for DW width $\Delta = 10$ nm calculated for different positions of the excitation region. (c) DW displacement taken 1 ps after the DW motion for different DW widths as a function of the excitation region position.

increases. The increasing trend persists up to a certain maximum value. This value is located for all studied DW widths at $z_{ex} \simeq \pm 20$ nm, which correspond to the cases when one of the borderlines of the excitation region is located at the initial position of the DW center $z = 0$. Small deviation of the extremes in the dependence shown in Fig. 6(c) from $z_{ex} = \pm 20$ nm might be caused by minor modification of the DW structure during the dynamics induced by nonhomogeneous spin currents. In this case, the asymmetry of right and left electron fluxes is maximal, which also maximizes the total spin-transfer torque acting on the DW, as shown in Fig. 4(d). We also find that when the distance of the excitation region becomes larger than $z_{ex} = l_{ex}/2$, the DW displacement decreases. This reduction of the DW displacement is related to the spin relaxation of the itinerant electrons which have to go through longer distances to reach the domain wall and contribute to the spin-transfer torque. Finally, the dependence of DW displacement on z_{ex} is an odd function, which depends on the direction of dominant flux of electrons passing the domain wall. If the excitation region position is shifted to the left (right) from the initial position of the DW center, the dominant electron flux contribution to the spin-transfer torque will be oriented to the right (left). Thus, the domain wall moves to the right (left) in agreement with the incident spin current.

VI. DISCUSSION

In Sec. IV we have studied a simplified model of a narrow magnetic domain wall. We find that our theoretical calculations are comparable to experimental observations and Monte Carlo simulations [25] showing a broadening of magnetic domain walls on a femtosecond timescale. This model was, however, restricted to collinear magnetic moments and therefore spin-transfer torques could not be analyzed.

As a next step, in Sec. V we have focused on wider domain walls taking into account the details of the domain wall profile. In this case we have found an enhancement of demagnetization in the vicinity of the domain wall. Similarly, as in the case of a narrow domain wall, the demagnetization effect is caused by the transfer of superdiffusive hot electrons between magnetic domains of opposite magnetization direction. In real 3-dimensional samples, this effect should appear on top of other processes leading to ultrafast demagnetization as a modification of the domain wall profile, which appears on a timescale of a few hundred femtoseconds. The second effect studied here is the generation of a spin-transfer torque due to a femtosecond laser pulse focused on a narrow part of the sample close to the domain wall. We could show that when the area excited by the laser pulse is asymmetric with respect to the domain wall center, the interaction of the hot electrons with the magnetization gradient can create a directed spin-transfer torque strong enough to induce domain wall motion. Due to the transient nature of the superdiffusive spin currents the spin-transfer torque acts only within less than 1 ps. The resulting DW displacement is not large, $\sim$3.5 nm (Fig. 6), yet it takes place very fast, which hence implies a significant rapidly changing out-of-equilibirum DW velocity, whose average value over the first 250 fs is $\sim 1.4 \times 10^4$ m/s (for $z_{\mathrm{ex}} =$ 30 nm). This value exceeds substantially currently known DW velocities. For example, high DW velocities ($\sim$750 m/s) have so far only been reported for synthetic antiferromagnets [7].

In our model we assumed a square excitation area of constant size comparable to the DW width. Our simulations show that the DW displacement is maximized when the edge of the excitation area falls on to the DW center. When the excitation area overlaps with the other half of the DW, a spin current in the opposite direction reduces the overall spin torque and decreases the DW shift. This suggests that the DW shift is maximized when the pulse decays abruptly across the DW, so that its effect on the other side of the DW is minimal. Thus, as small spatial smearing of the laser pulse profile as possible is favorable. Also, when we extend the size of the excitation area, the effect of electrons excited too far from the DW becomes negligible, since they loose their energy before reaching the DW. Hence the energy density of the beam near the DW (within tens of nm) rather than the total deposited energy is important here.

We further note that current or magnetic field induced DW motions have been studied under quasiequilibrium conditions, under which the DW velocity is limited, e.g., by the Walker breakdown limit [51] or, at higher DW velocities, by magnonic or phononic barriers [64–67]. This situation is, however, very different from our case, when the spin current is very inhomogeneous in space and rapidly changes in time. The DW center displacement takes place in a short time period; however, the displacement is smaller than the DW width.

Despite the qualitative agreement with experimental results, it is at this point relevant to mention the assumptions considered in our model and the constraints they impose on the magnetization dynamics due to spin transfer. Currents of superdiffusive hot electrons persist in the sample for about 500 fs [20]. This is the timescale of the demagnetization process and spin-transfer torque action. The question is how these effects can finally influence the resulting magnetization dynamics. First, the partial ultrafast demagnetization, which happens on the same timescale as the spin-transfer torque, influences just the magnitude of the magnetization. In our calculations, e.g., for a 10 nm domain wall width, this effect is about 15% and it strongly decreases with the domain wall thickness. Importantly, the direction of magnetization remains unchanged. Note that for a reduced magnetization the torque actually causes a bigger change in the magnetization. The inhomogeneous variation of magnetization length, $M(z)$, can induce changes in the local effective magnetic field and, consequently, magnetization dynamics can occur. However, this magnetization dynamics in the local magnetic field has typically a timescale of a few nanoseconds [49]. Therefore, it is out of the scope of this work. Second, in our modeling of the magnetization dynamics we assumed that the domain wall motion does not influence the spin transport. This assumption is maybe more problematic since both domain wall motion and spin-transfer torque are mutually coupled and share the same timescale. Our argument is based on the length scale and on the smoothness of the domain wall profile. Namely, in the domain wall the magnetization is varying slowly. When the domain wall shifts by $\sim$3 nm, the generated spin torque is not substantially influenced by a minor change of local magnetic direction. More important for the modeling is the effect of relaxation of the hot electrons during the transport. Although the former effect is not taken into account in our simulations, the latter one is fully incorporated.

In addition, it deserves to be mentioned that a femtosecond laser pulse might be the source of other effects leading to domain wall motion, which are not included in our simulations, such as the entropic torque [68–70], which forces the domain wall to move toward the laser spot, and the magnonic torque [5,70,71] of thermally induced magnons that can influence the domain wall motion. Although the former is relatively strong, it leads to magnetization dynamics on a nanosecond timescale and domain wall velocities reach values of $\sim 10^2$ m/s [4]. Importantly, the direction of the entropic torque is opposite to the one induced by superdiffusive spin-dependent transport. On the other hand, the magnonic torque is relatively weak and leads to domain wall velocities on the order of only 10 m/s [4].

Lastly, a further aspect that becomes important for domain wall motion once the fast spin-transfer torque has ceased is the domain wall inertia (see, e.g., [11,72]), which we have not considered here. While the superdiffusive spin currents act only within 1 ps, these could provide a stimulus that enables depinning of domain walls [29] and initiate inertial domain wall motion.

Finally, we have studied a domain wall in a material with in-plane uniaxial magnetocrystalline anisotropy, where the

magnetization direction varies smoothly on a long length scale. Nevertheless, our model, with extensions for domain wall reflections, allows us also to study sharp magnetic domain walls of arbitrary profile, which can be observed in multilayers with strong perpendicular magnetic anisotropy [25–28].

VII. CONCLUSIONS

In summary, we have formulated a model describing 1-dimensional laser-generated transport of hot electrons through a magnetic domain wall and the spin dynamics it induces. Our study demonstrates both the contribution of the spin transport between magnetic domains of opposite spin direction to the ultrafast demagnetization as well as the possibility of spin torque generation. We have shown that when the laser beam is focused on a restricted area of the sample, it can create an imbalance between right and left flowing fluxes of hot electrons flowing through the domain wall. This leads to the nonzero total spin-transfer torque that can induce a shift of the domain wall by a few nanometers in about 500 fs. This mechanism of domain wall motion creates a relatively small shift compared to other laser-induced mechanisms, such as entropic [68–70] or magnonic [4] torques due to thermal magnons, when one looks at the situation tens of picoseconds after the pulse. However, a definite advantage is that it can be controlled by femtosecond laser pulses, and within the time window of less than a ps it provides very high DW velocities on the order of 10^4 m/s in a ferromagnetic system, which exceeds considerably the values of velocities of current-induced domain wall motion [59,73–75].

ACKNOWLEDGMENTS

This work was supported by the European Regional Development Fund in the IT4Innovations National Supercomputing Center Path to Exascale project (Project No. CZ.02.1.01/0.0/0.0/16_013/0001791) within the Operational Programme Research, Development, and Education, by the Czech Science Foundation (Grant No. 18-07172S), by the Swedish Research Council (VR), and by the K. and A. Wallenberg Foundation (Grant No. 2015.0060). The authors furthermore thank the Ministry of Education, Youth, and Sports for the Large Infrastructures for Research, Experimental Development, and Innovations project "IT4Innovations National Supercomputing Center LM2015070," as well as the Deutsche Forschungsgemeinschaft for financial support via RI 2891/1-1 and via the TRR 227, and the Swedish National Infrastructure for Computing (SNIC). We thank Ilja Turek and Jérôme Hurst for valuable discussions.

[1] J. C. Slonczewski, J. Magn. Magn. Mater. **159**, L1 (1996).
[2] L. Berger, Phys. Rev. B **54**, 9353 (1996).
[3] M. Hatami, G. E. W. Bauer, Q. Zhang, and P. J. Kelly, Phys. Rev. Lett. **99**, 066603 (2007).
[4] S. Moretti, V. Raposo, E. Martinez, and L. Lopez-Diaz, Phys. Rev. B **95**, 064419 (2017).
[5] D. Hinzke and U. Nowak, Phys. Rev. Lett. **107**, 027205 (2011).
[6] A. Manchon and S. Zhang, Phys. Rev. B **79**, 094422 (2009).
[7] S.-H. Yang, K.-S. Ryu, and S. Parkin, Nat. Nanotechnol. **10**, 221 (2015).
[8] S. S. P. Parkin, M. Hayashi, and L. Thomas, Science **320**, 190 (2008).
[9] E. Beaurepaire, J.-C. Merle, A. Daunois, and J.-Y. Bigot, Phys. Rev. Lett. **76**, 4250 (1996).
[10] P. Němec, E. Rozkotová, N. Tesarová, F. Trojánek, E. De Ranieri, K. Olejník, J. Zemen, V. Novák, M. Cukr, P. Malý, and T. Jungwirth, Nat. Phys. **8**, 411 (2012).
[11] T. Janda, P. E. Roy, R. M. Otxoa, Z. Šobáň, A. Ramsay, A. C. Irvine, F. Trojanek, M. Surýnek, R. P. Campion, B. L. Gallagher, P. Němec, T. Jungwirth, and J. Wunderlich, Nat. Commun. **8**, 15226 (2017).
[12] N. Tesarová, P. Němec, E. Rozkotová, J. Zemen, T. Janda, D. Butkovičová, F. Trojánek, K. Olejník, V. Novák, P. Malý, and T. Jungwirth, Nat. Photonics **7**, 492 (2013).
[13] B. Koopmans, G. Malinowski, F. Dalla Longa, D. Steiauf, M. Fähnle, T. Roth, M. Cinchetti, and M. Aeschlimann, Nat. Mater. **9**, 259 (2010).
[14] B. Y. Mueller, T. Roth, M. Cinchetti, M. Aeschlimann, and B. Rethfeld, New J. Phys. **13**, 123010 (2011).
[15] E. Carpene, E. Mancini, C. Dallera, M. Brenna, E. Puppin, and S. De Silvestri, Phys. Rev. B **78**, 174422 (2008).
[16] M. Krauß, T. Roth, S. Alebrand, D. Steil, M. Cinchetti, M. Aeschlimann, and H. C. Schneider, Phys. Rev. B **80**, 180407(R) (2009).
[17] T. Roth, A. J. Schellekens, S. Alebrand, O. Schmitt, D. Steil, B. Koopmans, M. Cinchetti, and M. Aeschlimann, Phys. Rev. X **2**, 021006 (2012).
[18] K. Carva, M. Battiato, and P. M. Oppeneer, Phys. Rev. Lett. **107**, 207201 (2011).
[19] M. Battiato, K. Carva, and P. M. Oppeneer, Phys. Rev. Lett. **105**, 027203 (2010).
[20] M. Battiato, K. Carva, and P. M. Oppeneer, Phys. Rev. B **86**, 024404 (2012).
[21] D. Rudolf, C. La-O-Vorakiat, M. Battiato, R. Adam, J. M. Shaw, E. Turgut, P. Maldonado, S. Mathias, P. Grychtol, H. T. Nembach, T. J. Silva, M. Aeschlimann, H. C. Kapteyn, M. M. Murnane, C. M. Schneider, and P. M. Oppeneer, Nat. Commun. **3**, 1037 (2012).
[22] A. J. Schellekens, K. C. Kuiper, R. R. J. C. de Wit, and B. Koopmans, Nat. Commun. **5**, 4333 (2014).
[23] G.-M. Choi, B.-C. Min, K.-J. Lee, and D. G. Cahill, Nat. Commun. **5**, 4334 (2014).
[24] I. Razdolski, A. Alekhin, N. Ilin, J. P. Meyburg, V. Roddatis, D. Diesing, U. Bovensiepen, and A. Melnikov, Nat. Commun. **8**, 15007 (2017).
[25] B. Pfau, S. Schaffert, L. Müller, C. Gutt, A. Al-Shemmary, F. Büttner, R. Delaunay, S. Düsterer, S. Flewett, R. Frömter, J. Geilhufe, E. Guehrs, C. Günther, R. Hawaldar, M. Hille, N. Jaouen, A. Kobs, K. Li, J. Mohanty, H. Redlin, W. Schlotter, D. Stickler, R. Treusch, B. Vodungbo, M. Kläui, H. P. Oepen, J. Lüning, G. Grübel, and S. Eisebitt, Nat. Commun. **3**, 1100 (2012).

[26] B. Vodungbo, J. Gautier, G. Lambert, A. B. Sardinha, M. Lozano, S. Sebban, M. Ducousso, W. Boutu, K. Li, B. Tudu, M. Tortarolo, R. Hawaldar, R. Delaunay, V. López-Flores, J. Arabski, C. Boeglin, H. Merdji, P. Zeitoun, and J. Lüning, Nat. Commun. **3**, 999 (2012).

[27] N. Moisan, G. Malinowski, J. Mauchain, M. Hehn, B. Vodungbo, J. Lüning, S. Mangin, E. E. Fullerton, and A. Thiaville, Sci. Rep. **4**, 4658 (2014).

[28] Y. Quessab, R. Medapalli, M. S. El Hadri, M. Hehn, G. Malinowski, E. E. Fullerton, and S. Mangin, Phys. Rev. B **97**, 054419 (2018).

[29] O. Sandig, Y. A. Shokr, J. Vogel, S. Valencia, F. Kronast, and W. Kuch, Phys. Rev. B **94**, 054414 (2016).

[30] Y. A. Shokr, O. Sandig, M. Erkovan, B. Zhang, M. Bernien, A. A. Ünal, F. Kronast, U. Parlak, J. Vogel, and W. Kuch, Phys. Rev. B **99**, 214404 (2019).

[31] T. Eggebrecht, M. Möller, J. G. Gatzmann, N. Rubiano da Silva, A. Feist, U. Martens, H. Ulrichs, M. Münzenberg, C. Ropers, and S. Schäfer, Phys. Rev. Lett. **118**, 097203 (2017).

[32] M. L. M. Lalieu, R. Lavrijsen, and B. Koopmans, Nat. Commun. **10**, 110 (2019).

[33] B. Zhang, Y. Xu, W. Zhao, D. Zhu, X. Lin, M. Hehn, G. Malinowski, D. Ravelosona, and S. Mangin, Phys. Rev. Appl. **11**, 034001 (2019).

[34] M. Battiato, P. Maldonado, and P. M. Oppeneer, J. Appl. Phys. **115**, 172611 (2014).

[35] R. Moreno, R. F. L. Evans, S. Khmelevskyi, M. C. Muñoz, R. W. Chantrell, and O. Chubykalo-Fesenko, Phys. Rev. B **94**, 104433 (2016).

[36] J. C. Slonczewski, J. Magn. Magn. Mater. **126**, 374 (1993).

[37] D. M. Edwards, R. P. Erickson, J. Mathon, R. B. Muniz, and M. Villeret, Mater. Sci. Eng. B **31**, 25 (1995).

[38] N. Bergeard, M. Hehn, S. Mangin, G. Lengaigne, F. Montaigne, M. L. M. Lalieu, B. Koopmans, and G. Malinowski, Phys. Rev. Lett. **117**, 147203 (2016).

[39] A. Eschenlohr, L. Persichetti, T. Kachel, M. Gabureac, P. Gambardella, and C. Stamm, J. Phys.: Condens. Matter **29**, 384002 (2017).

[40] M. L. M. Lalieu, M. J. G. Peeters, S. R. R. Haenen, R. Lavrijsen, and B. Koopmans, Phys. Rev. B **96**, 220411(R) (2017).

[41] M. Hofherr, P. Maldonado, O. Schmitt, M. Berritta, U. Bierbrauer, S. Sadashivaiah, A. J. Schellekens, B. Koopmans, D. Steil, M. Cinchetti, B. Stadtmüller, P. M. Oppeneer, S. Mathias, and M. Aeschlimann, Phys. Rev. B **96**, 100403(R) (2017).

[42] G. Malinowski, N. Bergeard, M. Hehn, and S. Mangin, Eur. Phys. J. B **91**, 98 (2018).

[43] D. M. Nenno, S. Kaltenborn, and H. C. Schneider, Phys. Rev. B **94**, 115102 (2016).

[44] J. C. Slonczewski, J. Magn. Magn. Mater. **247**, 324 (2002).

[45] M. D. Stiles and A. Zangwill, Phys. Rev. B **66**, 014407 (2002).

[46] D. C. Ralph and M. D. Stiles, J. Magn. Magn. Mater. **320**, 1190 (2008).

[47] T. Valet and A. Fert, Phys. Rev. B **48**, 7099 (1993).

[48] J. Barnaś, A. Fert, M. Gmitra, I. Weymann, and V. K. Dugaev, Phys. Rev. B **72**, 024426 (2005).

[49] D. Berkov and J. Miltat, J. Magn. Magn. Mater. **320**, 1238 (2008).

[50] P. Baláž, M. Žonda, K. Carva, P. Maldonado, and P. M. Oppeneer, J. Phys.: Condens. Matter **30**, 115801 (2018).

[51] N. L. Schryer and L. R. Walker, J. Appl. Phys. **45**, 5406 (1974).

[52] G. Tatara, H. Kohno, and J. Shibata, Phys. Rep. **468**, 213 (2008).

[53] Z. Li and S. Zhang, Phys. Rev. Lett. **92**, 207203 (2004).

[54] A. Ghosh, S. Auffret, U. Ebels, and W. E. Bailey, Phys. Rev. Lett. **109**, 127202 (2012).

[55] P. Bruno, Phys. Rev. Lett. **83**, 2425 (1999).

[56] V. K. Dugaev, J. Berakdar, and J. Barnaś, Phys. Rev. B **68**, 104434 (2003).

[57] R. Sýkora and I. Turek, Acta Phys. Polonica A **113**, 15 (2008).

[58] G. Tatara and H. Kohno, Phys. Rev. Lett. **92**, 086601 (2004).

[59] Z. Li and S. Zhang, Phys. Rev. B **70**, 024417 (2004).

[60] V. K. Dugaev, J. Barnaś, A. Łusakowski, and Ł. A. Turski, Phys. Rev. B **65**, 224419 (2002).

[61] V. P. Zhukov and E. V. Chulkov, Phys. Solid State **51**, 2211 (2009).

[62] V. P. Zhukov, E. V. Chulkov, and P. M. Echenique, Phys. Status Solidi (a) **205**, 1296 (2008).

[63] G. S. D. Beach, M. Tsoi, and J. L. Erskine, J. Magn. Magn. Mater. **320**, 1272 (2008).

[64] M. Yan, A. Kákay, S. Gliga, and R. Hertel, Phys. Rev. Lett. **104**, 057201 (2010).

[65] M. Yan, C. Andreas, A. Kákay, F. Garcia-Sanchez, and R. Hertel, Appl. Phys. Lett. **99**, 122505 (2011).

[66] S. Selzer, U. Atxitia, U. Ritzmann, D. Hinzke, and U. Nowak, Phys. Rev. Lett. **117**, 107201 (2016).

[67] V. G. Bar'yakhtar, M. V. Chetkin, B. A. Ivanov, and S. N. Gadetskii, *Dynamics of Topological Magnetic Solitons: Experiment and Theory* (Springer, Berlin, 1994).

[68] F. Schlickeiser, U. Ritzmann, D. Hinzke, and U. Nowak, Phys. Rev. Lett. **113**, 097201 (2014).

[69] X. S. Wang and X. R. Wang, Phys. Rev. B **90**, 014414 (2014).

[70] S. K. Kim and Y. Tserkovnyak, Phys. Rev. B **92**, 020410(R) (2015).

[71] P. Yan, X. S. Wang, and X. R. Wang, Phys. Rev. Lett. **107**, 177207 (2011).

[72] L. Thomas, R. Moriya, C. Rettner, and S. S. P. Parkin, Science **330**, 1810 (2010).

[73] D. Claudio-Gonzalez, A. Thiaville, and J. Miltat, Phys. Rev. Lett. **108**, 227208 (2012).

[74] J.-Y. Lee, K.-S. Lee, and S.-K. Kim, Appl. Phys. Lett. **91**, 122513 (2007).

[75] A. Thiaville, Y. Nakatani, J. Miltat, and Y. Suzuki, Europhys. Lett. **69**, 990 (2005).